

RESEARCH ARTICLE

10.1029/2018JA025517

Explicit IMF  $B_y$  Dependence in High-Latitude Geomagnetic Activity

Special Section:

The Earth's Magnetosphere: New Tools, New Thinking, New Results

L. Holappa<sup>1,2,3</sup> and K. Mursula<sup>1</sup>

<sup>1</sup>ReSoLVE Centre of Excellence, Space Climate Research Unit, University of Oulu, Oulu, Finland, <sup>2</sup>Solar Physics Laboratory, NASA Goddard Space Flight Center, Greenbelt, MD, USA, <sup>3</sup>Department of Physics, The Catholic University of America, Washington, DC, USA

Key Points:

- IMF  $B_y$  is an explicit driver of high-latitude geomagnetic activity
- High-latitude geomagnetic activity is suppressed in local winter for  $B_y < 0$  in Northern Hemisphere and for  $B_y > 0$  in Southern Hemisphere
- Explicit  $B_y$  effect maximizes when the Earth's dipole axis points toward night

Correspondence to:

L. Holappa, lauri.holappa@oulu.fi

Citation:

Holappa, L., & Mursula, K. (2018). Explicit IMF  $B_y$  dependence in high-latitude geomagnetic activity. *Journal of Geophysical Research: Space Physics*, 123. <https://doi.org/10.1029/2018JA025517>

Received 26 MAR 2018

Accepted 14 MAY 2018

Accepted article online 21 MAY 2018

**Abstract** The interaction of the solar wind with the Earth's magnetic field produces geomagnetic activity, which is critically dependent on the orientation of the interplanetary magnetic field (IMF). Most solar wind coupling functions quantify this dependence on the IMF orientation with the so-called IMF clock angle in a way, which is symmetric with respect to the sign of the  $B_y$  component. However, recent studies have suggested that the sign of  $B_y$  is an additional, independent driver of high-latitude geomagnetic activity, leading to higher (weaker) geomagnetic activity in Northern Hemisphere (NH) winter for  $B_y > 0$  ( $B_y < 0$ ). In this paper we quantify the size of this explicit  $B_y$  effect with respect to the solar wind coupling function, both for northern and southern high-latitude geomagnetic activity. We show that high-latitude geomagnetic activity is significantly (by about 40%–50%) suppressed for  $B_y < 0$  in NH winter and for  $B_y > 0$  in Southern Hemisphere winter. When averaged over all months, high-latitude geomagnetic activity in NH is about 12% weaker for  $B_y < 0$  than for  $B_y > 0$ . The  $B_y$  effect affects the westward electrojet strongly, but hardly at all the eastward electrojet. We also show that the suppression of the westward electrojet in NH during  $B_y < 0$  maximizes when the Earth's dipole axis points toward the night sector, that is, when the auroral region is maximally in darkness.

1. Introduction

The interaction of the solar wind and the interplanetary magnetic field (IMF) with the terrestrial magnetic field generates geomagnetic activity and various other phenomena in the near-Earth space. One of the main goals of solar-terrestrial physics is to understand the details of the different physical processes involved in this interaction. A better theoretical understanding of this interaction will allow, for example, for a better prediction of geomagnetic activity and related space weather hazards, such as the charging and loss of satellites and geomagnetically induced currents in power lines.

The most important parameter for solar wind-magnetosphere coupling is the north-south ( $B_z$ ) component of the IMF in the geocentric solar magnetospheric (GSM) coordinate system, which controls magnetic reconnection at the subsolar magnetopause (Dungey, 1961). Accordingly, IMF  $B_z$  is the key parameter also for geomagnetic activity and is included in different solar wind-magnetosphere coupling functions, such as the Kan-Lee electric field  $E_{KL} = vB_T^2 \sin^2(\theta/2)$  (Kan & Lee, 1979) and the Newell universal coupling function  $d\Phi_{MP}/dt = v^{4/3} B_T^{2/3} \sin^{8/3}(\theta/2)$  (Newell et al., 2007). In these expressions  $v$  is solar wind speed,  $B_T = \sqrt{B_z^2 + B_y^2}$ , and  $\theta = \arctan(B_y/B_z)$  is the so-called clock angle. The same clock angle dependence as in  $E_{KL}$  also appears in the recently developed Borovsky coupling function (Borovsky & Birn, 2014). Note that IMF  $B_y$  is included in these coupling functions, but its effect is independent on its polarity (sign), due to the symmetry of factors appearing in  $B_T$  and  $\theta$ . In this paper we use the Newell universal coupling function because it is optimized for high-latitude geomagnetic indices, such as the AL index (Davis & Sugiura, 1966), which primarily measures the westward electrojet in the Northern Hemisphere (NH). However, the main results of this paper do not depend on the choice of the coupling function.

While the polarity of IMF  $B_y$  does not have any independent role in the solar wind-magnetosphere coupling functions, it plays a significant role in modulating the IMF  $B_z$  component observed in the GSM coordinate system via the Russell-McPherron (RMP) effect (Russell & McPherron, 1973). The RMP effect arises due to the

seasonally (and diurnally) changing angle between the solar equatorial plane and the GSM  $z$  axis. During spring (fall) an equatorial IMF vector pointing toward (away from) the Sun has a southward  $B_z$  component in the GSM coordinate system, which enhances geomagnetic activity at this time. This effect is included in the solar wind-magnetosphere coupling functions. Note also that the RMP effect maximizes on 5 April and 5 October; that is, the maximum effect is shifted from the equinoxes toward the following solstices.

There are also some magnetospheric and ionospheric phenomena for which the polarity of IMF  $B_y$  plays an independent role. For example, Svalgaard (1968) and Mansurov (1969) showed that the daily variation of the magnetic field at high latitudes depends on the IMF sector polarity. Friis-Christensen et al. (1972) showed that this Svalgaard-Mansurov effect is due to the  $B_y$  component of the IMF ( $B_x$  being insignificant). Later studies using ground-based magnetic field observations (Friis-Christensen et al., 1985) and radar measurements (Pettigrew et al., 2010; Ruohoniemi & Greenwald, 1996, 2005) have shown that IMF  $B_y$  controls the shape of polar cap convection pattern and the amplitude of the cross-polar cap potential.

Recently, Laundal et al. (2016) and Friis-Christensen et al. (2017) showed that there is a seasonally dependent effect of the IMF  $B_y$  polarity in the  $AL$  index. They found that in NH winter (NH summer)  $|AL|$  is greater (smaller) under  $B_y > 0$  than under  $B_y < 0$ . This is partly supported by Smith et al. (2017), who showed that the auroral electrojet currents (not differentiating westward or eastward electrojets), derived from observations of different polar-orbiting satellites, are enhanced in NH winter for  $B_y > 0$  and in the Southern Hemisphere (SH) winter for  $B_y < 0$ . However, Smith et al. (2017) did not find significant  $B_y$  polarity effect in the summer hemisphere.

In this paper we perform a detailed study on the effect of IMF  $B_y$  to the high-latitude geomagnetic activity using geomagnetic indices from both hemispheres. We will show that the RMP effect can lead to a significant bias in any statistical studies quantifying the effect of  $B_y$ , if not properly accounted for. We will show that there is a strong, seasonally varying *explicit*  $B_y$  dependence, which is not due to the RMP effect and which is not included in the coupling functions that describe the interaction between solar wind and geomagnetic activity (but do include, e.g., the RMP effect). The paper is organized as follows. Section 2 gives details of different databases and geomagnetic indices used in this paper. In sections 3 and 4 we study the effect of IMF  $B_y$  to the  $AL$  and  $AU$  indices, respectively. In section 5 we study the universal time (UT) dependence of the  $B_y$  effect, and in section 6 the  $B_y$  effect in the SH using the  $K$  index of the Syowa station. In section 7 we study possible biases to our results caused by IMF  $B_x$  component. Finally, we discuss our results and give our conclusions in section 8.

## 2. Data

In this paper we use the hourly mean values of solar wind speed and the different IMF components in 1966–2015 from the OMNI2 database (<https://omniweb.gsfc.nasa.gov/>) time shifted to the Earth's orbit, and the hourly  $AL$  and  $AU$  indices in 1966–2015 as proxies of high-latitude geomagnetic activity in the NH. The  $AL$  and  $AU$  indices are defined as the momentarily lowest ( $AL$ ) and highest ( $AU$ ) deviations in the horizontal magnetic field measured by a network of 12 stations at geomagnetic latitudes ranging from 60°N to 71°N. The  $AL$  and  $AU$  indices are proxies for the intensities of the westward and eastward electrojets in the NH, respectively.

Due to the small number of long-running magnetic stations at southern high latitudes, there are no equivalents of  $AL$  or  $AU$  indices available for the SH. In this paper we use the geomagnetic  $K$  index measured at the Japanese Syowa station in 1966–2015 (geographic coordinates 69.0°S, 39.5°E; corrected geomagnetic coordinates: 65.6°S, 118°E). This is the longest-running geomagnetic index measured at a site, which is located in the proximity of the southern auroral electrojets.

## 3. $AL$ Index and Solar Wind Coupling Functions for Positive and Negative $B_y$

Figure 1 shows the superposed monthly averages of the Newell universal coupling function  $d\Phi_{MP}/dt$  separately for  $B_y > 0$  (away from the Sun) and  $B_y < 0$  (toward the Sun) conditions in 1966–2015. The polarity of  $B_y$  is defined in GSM coordinates in Figure 1a and in geocentric solar equatorial (GSE) coordinates in Figure 1b. However,  $d\Phi_{MP}/dt$  is calculated in the GSM coordinates in both Figures 1a and 1b. Figure 1 verifies the well-known,  $B_y$ -dependent seasonal variation, with maxima in  $d\Phi_{MP}/dt$  in spring for  $B_y < 0$  and in fall for  $B_y > 0$  conditions. This is in agreement with the RMP effect, according to which, a toward (away) oriented field line attains an enhanced southward component in the GSM frame in spring (fall). Because a typical IMF field

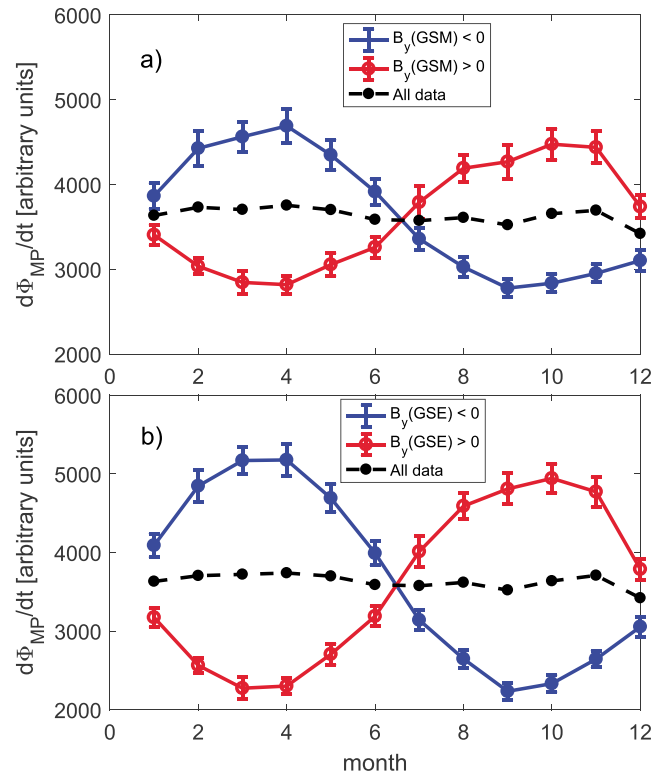


**Figure 1.** Superposed monthly averages of the Newell universal coupling function  $d\Phi_{MP}/dt$  in GSM coordinate system for the two polarities of IMF  $B_y$ . The polarity of IMF  $B_y$  is defined in GSM coordinates in panel (a) and in GSE coordinates in panel (b). Standard errors of the superposed monthly averages are denoted by vertical bars. IMF = interplanetary magnetic field; GSM = geocentric solar magnetospheric; GSE = geocentric solar equatorial.

line lies close to the ecliptic plane ( $xy$  plane in GSE coordinates), defining the sign of  $B_y$  in GSE coordinates yields a stronger seasonal variation in Figure 1b than in Figure 1a.

Figure 2 shows the superposed monthly averages of the  $|AL|$  index for the two  $B_y$  polarities, with the sector division made in the two coordinate systems. As the solar wind driver  $d\Phi_{MP}/dt$ , also the  $AL$  index exhibits maxima in spring for  $B_y < 0$  and in fall for  $B_y > 0$ , with the same peak months (April and in October) as in Figure 1. As noted above, April and October are the months of the maximum effect of the RMP mechanism.

There are, however, significant differences between the seasonal patterns of  $d\Phi_{MP}/dt$  and the  $AL$  index. While the peaks and, especially, the minima of  $d\Phi_{MP}/dt$  (Figure 1) are roughly equal for the two polarities of  $B_y$ , the minimum of the  $|AL|$  index (Figure 2) in winter for  $B_y < 0$  is much lower than the minimum in spring/summer for  $B_y > 0$ . There are actually five consecutive months (September–January) during which  $|AL(B_y < 0)|$  is below any of the superposed monthly values of  $|AL(B_y > 0)|$ . Thus, the fall-winter response of  $|AL|$  to solar wind driving for  $B_y < 0$  conditions is considerably weaker than that expected from the seasonal distribution of the solar wind driver function.

Because the seasonal patterns in Figures 1 and 2 are primarily due to the RMO effect, Figure 2 includes the RMP modulation of the strength of solar wind driving via the  $B_y$ -symmetric clock angle. To separate the possible explicit  $B_y$  effect on the  $AL$  index, we study the response of  $AL$  to  $B_y$  during given values of the solar wind driver function. Figure 3 shows the average values of  $|AL|$  in 1966–2015 for different measured values of  $B_y(\text{GSM})$  and  $d\Phi_{MP}/dt$  around winter solstice (21 December  $\pm$  15 days). Figure 3 shows a clear asymmetry in the response of the  $AL$  index to  $B_y(\text{GSM})$ : for a given value of  $d\Phi_{MP}/dt$ ,  $|AL|$  increases with increasing  $B_y(\text{GSM})$ . An opposite, but slightly weaker  $B_y$  dependence can be seen in Figure 4 around the summer solstice (21 June  $\pm$  15 days). Thus, there is an explicit  $B_y$  dependence in  $|AL|$ , which suppresses  $|AL|$  for  $B_y < 0$  in NH winter and for  $B_y > 0$  in NH summer.

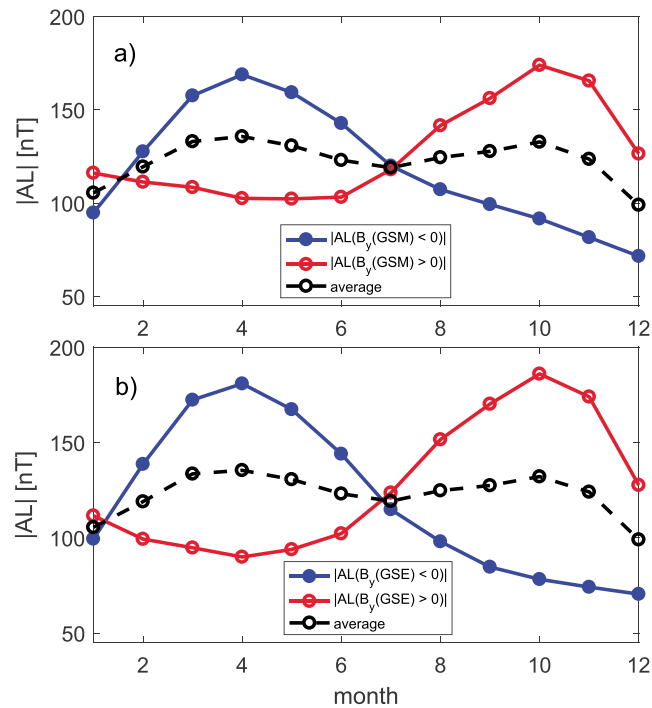


**Figure 2.** Superposed monthly averages of the  $|AL|$  index for the two polarities of IMF  $B_y$ . The polarity of IMF  $B_y$  is defined in GSM coordinates in panel (a) and in GSE coordinates in panel (b). IMF = interplanetary magnetic field; GSM = geocentric solar magnetospheric; GSE = geocentric solar equatorial.

Figures 5 and 6 show the average  $|AL|$  as a function of  $B_y(\text{GSM})$  and  $d\Phi_{\text{MP}}/dt$  around spring and fall equinoxes ( $20 \text{ March} \pm 15 \text{ days}$  and  $22 \text{ September} \pm 15 \text{ days}$ , respectively). In spring the dependence of  $|AL|$  for a given value of  $d\Phi_{\text{MP}}/dt$  is quite symmetric with respect to the sign of  $B_y$ . Only very large  $B_y > 0$  values lead to suppressed  $|AL|$ . (Because this is only seen for one polarity of  $B_y$ , there is no saturation of  $AL$  for large values of  $|B_y|$ .) However, Figure 6 shows a weak but quite systematic increase of  $|AL|$  with  $B_y$  in fall, in analogy to Figure 3.

In principle, the  $B_y$  effect seen, for example, in winter (see Figure 3) might well be due either to the enhancement of the  $|AL|$  index for  $B_y > 0$  or to the suppression of  $|AL|$  for  $B_y < 0$ . To study this further, we show

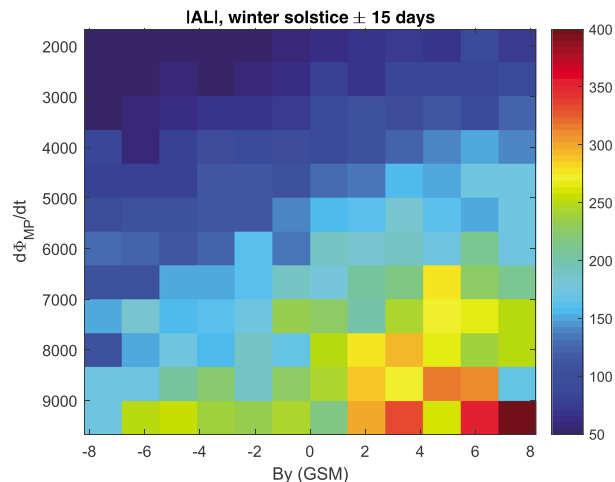


**Figure 3.** Averages of  $|AL|$  in 1966–2015 (in color code) during different values of  $d\Phi_{\text{MP}}/dt$  and  $B_y$ . Only data within  $\pm 15$  days from the NH winter solstice (21 December) are included. GSM = geocentric solar magnetospheric.

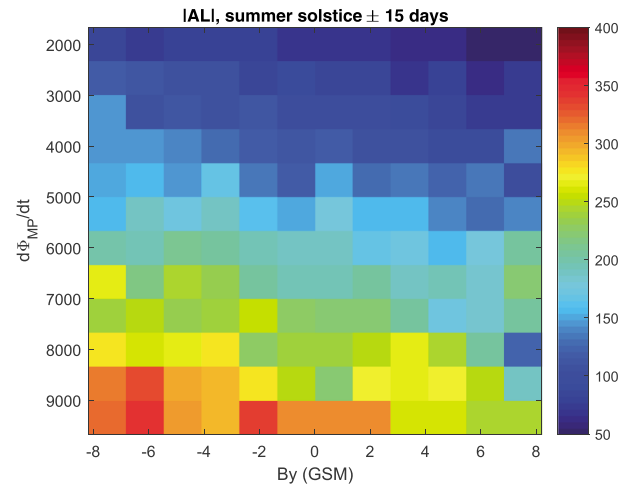


**Figure 4.** Averages of  $|AL|$  in 1966–2015 (in color code) during different values of  $d\Phi_{MP}/dt$  and  $B_y$ . Only data within  $\pm 15$  days from the Northern Hemisphere summer solstice (21 June) are included. GSM = geocentric solar magnetospheric.

in Figure 7 the ratios between the measured and predicted values of the  $|AL|$  index

$$R^+(AL) = \frac{|AL(B_y > 0)|}{|a \cdot d\Phi_{MP}/dt(B_y > 0) + b|} \quad (1)$$

$$R^-(AL) = \frac{|AL(B_y < 0)|}{|a \cdot d\Phi_{MP}/dt(B_y < 0) + b|} \quad (2)$$

where the coefficients  $a = 0.024 \text{ nT}^{1/3}/(\text{km/s})^{4/3}$  and  $b = 12.3 \text{ nT}$  are obtained from the linear least squares fit using all hourly solar wind and  $AL$  data in 1966–2015 without  $B_y$  separation. Figure 7 shows that the ratio  $R^-(AL)$  is significantly below 1 in winter months, reaching the minimum of 0.67 in December. On the contrary,  $R^+ \approx 1$  in winter months. This proves that the explicit  $B_y$  effect *suppresses* geomagnetic activity for  $B_y < 0$  in winter rather than enhances it for  $B_y > 0$ . The remaining semiannual variation in  $R^+(AL)$  is probably mostly due to the so-called equinoctial effect (Cliver et al., 2000; Lyatsky et al., 2001), which modulates the relation between the solar wind driver and geomagnetic activity.

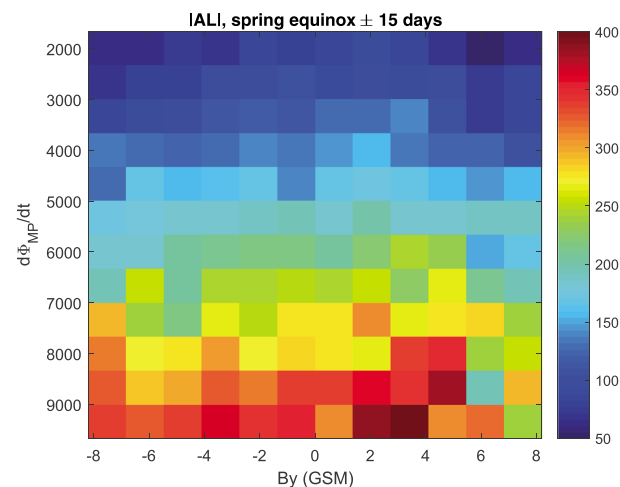


**Figure 5.** Averages of  $|AL|$  in 1966–2015 (in color code) during different values of  $d\Phi_{MP}/dt$  and  $B_y$ . Only data within  $\pm 15$  days from the Northern Hemisphere spring equinox (20 March) are included. GSM = geocentric solar magnetospheric.

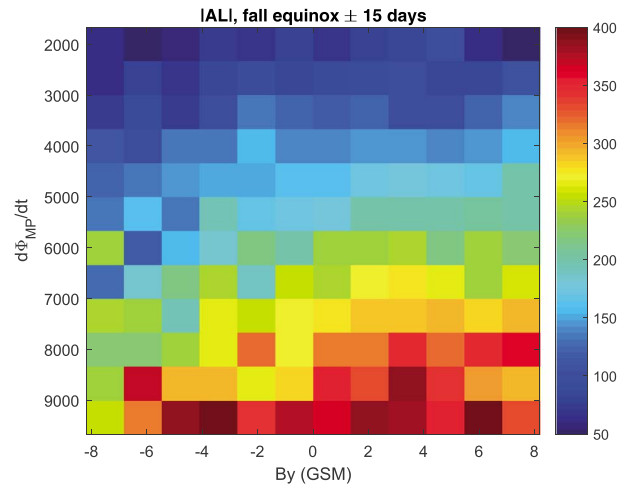


**Figure 6.** Averages of  $|AL|$  in 1966–2015 (in color code) during different values of  $d\Phi_{MP}/dt$  and  $B_y$ . Only data within  $\pm 15$  days from the Northern Hemisphere fall equinox (22 September) are included. GSM = geocentric solar magnetospheric.

To further quantify the strength of the explicit  $B_y$  effect in the  $AL$  index, we define the ratio

$$R_{\text{meas}}^{+/-}(AL) = \frac{|AL(B_y > 0)|}{|AL(B_y < 0)|} \quad (3)$$

calculated from the measured values of  $|AL|$  and the corresponding ratio predicted from the solar wind driver function

$$R_{\text{pred}}^{+/-}(AL) = \frac{a \cdot d\Phi_{MP}/dt(B_y > 0) + b}{a \cdot d\Phi_{MP}/dt(B_y < 0) + b} \quad (4)$$

These ratios are shown in Figure 8a. While  $R_{\text{meas}}^{+/-}(AL)$  and  $R_{\text{pred}}^{+/-}(AL)$  show qualitatively similar seasonal variations, there are some significant differences. In particular, as expected from the comparison of Figures 1 and 2 and Figure 7,  $R_{\text{meas}}^{+/-}$  attains significantly higher values than  $R_{\text{pred}}^{+/-}$  in October, November, December, and January. Interestingly,  $R_{\text{meas}}^{+/-} > 1$  even in January, when the RMP effect already favors  $B_y < 0$ , leading to  $R_{\text{pred}}^{+/-} < 1$ . This strongly implies that the winter minimum of  $|AL(B_y < 0)|$  is a major effect in high-latitude geomagnetic activity, which is not due to the RMP effect.

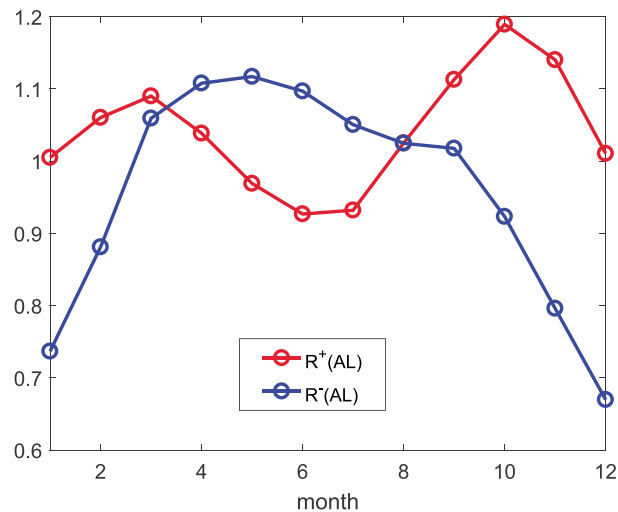


**Figure 7.** Ratios of measured and predicted values of the  $|AL|$  index for  $B_y > 0$  and  $B_y < 0$  [ $R^+(AL)$  and  $R^-(AL)$ , respectively; see equations (3) and (4)].

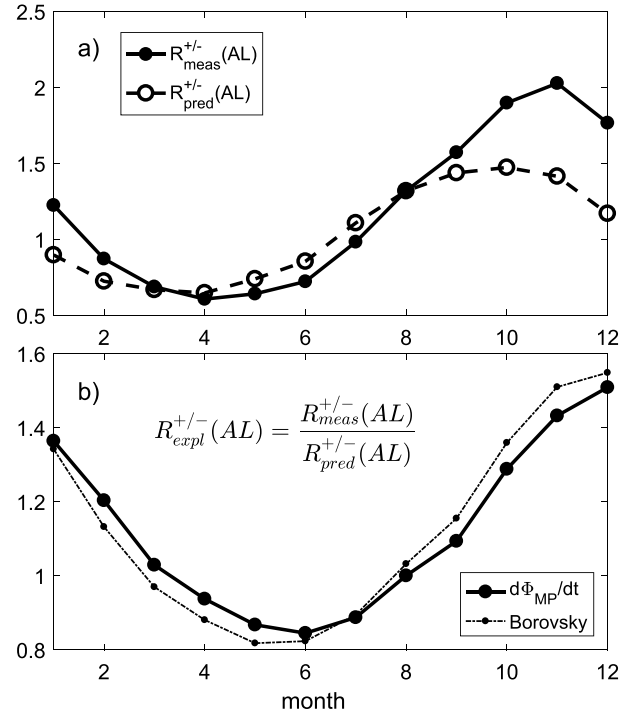


**Figure 8.** (a) Measured ( $R_{meas}^{+/-}$ ) and predicted ( $R_{pred}^{+/-}$ ) ratios of  $|AL(B_y > 0)|/|AL(B_y < 0)|$ . (b) Ratio of measured and predicted ratios  $R_{expl}^{+/-} = R_{meas}^{+/-}(AL)/R_{pred}^{+/-}(AL)$ . Ratio  $R_{expl}^{+/-}$  is calculated for  $d\Phi_{MP}/dt$  and the Borovsky coupling function.

Figure 8b shows the ratio of ratios

$$R_{expl}^{+/-}(AL) = \frac{R_{meas}^{+/-}(AL)}{R_{pred}^{+/-}(AL)}, \quad (5)$$

which maximizes in winter and minimizes in summer. For this plot we have included also the similar ratio  $R_{expl}^{+/-}(AL)$  calculated using the Borovsky coupling function (Borovsky & Birn, 2014), yielding a very similar result as  $d\Phi_{MP}/dt$ . This gives confidence that the results obtained in this paper are not limited to one specific coupling function. (Note also that even the clock angle dependencies are somewhat different in Newell and Borovsky functions.) The ratio  $R_{expl}^{+/-}$  quantifies the strength of the explicit  $B_y$  effect by removing not only the RMP effect but also other known causes of seasonal variation, like the equinoctial effect. Note also that the maximum and the minimum of the ratio  $R_{expl}^{+/-}(AL)$  occur exactly at summer and winter solstices. This (together with Figure 7) indicates that the response of the westward electrojet (of the NH) to solar wind driving is considerably weaker in winter but slightly stronger in summer for  $B_y < 0$  than for  $B_y > 0$ . Averaging  $R_{expl}^{+/-}(AL)$  over all 12 months yields to the overall average of 1.12. Thus, the overall annual response of the westward electrojet to solar wind driving is 12% weaker for  $B_y < 0$  than for  $B_y > 0$ . During the winter months (November–January) the ratio  $R_{expl}^{+/-}(AL)$  is 1.44, indicating a highly significant effect.

#### 4. AU Index for Positive and Negative $B_y$

Figure 9 shows the superposed monthly averages of the AU index for the two IMF  $B_y$  polarities in 1966–2015. The AU index shows a very strong annual (summer–winter) variation, related to varying illumination of the ionosphere (see, e.g., Finch et al., 2008) which can be seen in the overall average of AU (also included in Figure 9). The seasonal variation of illumination strongly affects AU because the intensity of eastward electrojet maximizes at the afternoon sector, where ionospheric conductivity is dominated by solar EUV radiation. Figure 9 shows that the IMF  $B_y$  component shifts the annual maximum of AU to May for  $B_y < 0$  and to August for  $B_y > 0$ , that is, always toward the corresponding RMP month (April and October, respectively).

Figure 10a shows the measured ratio  $R_{meas}^{+/-}(AU) = AU(B_y > 0)/AU(B_y < 0)$  and the corresponding predicted ratio  $R_{pred}^{+/-}(AU)$  calculated in the same way as for the AL index above (now  $a = 0.0129 \text{ nT}^{1/3}/(\text{km/s})^{4/3}$

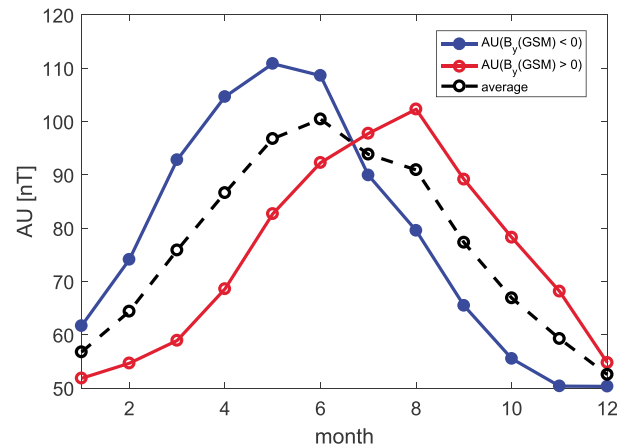


**Figure 9.** Averages of the  $AU$  index under different polarities of interplanetary magnetic field  $B_y$  as a function of month. GSM = geocentric solar magnetospheric.

and  $b = 29.7$  nT). Unlike for the  $AL$  index,  $R_{meas}^{+/-}(AU)$  and  $R_{pred}^{+/-}(AU)$  are very similar and their ratio  $R_{expl}^{+/-}(AU)$  depicted in Figure 10b remains close to one for all months. (The overall mean of  $R_{expl}^{+/-}(AU)$  is 0.97.) Note how closely Figure 10a reproduces the seasonal pattern of the RMP effect. This proves that the RMP effect plays almost an exclusive role in varying the seasonal variation of the  $AU$  index with IMF  $B_y$  polarity (Figure 9). Thus, the  $AU$  index does not have any notable explicit dependence on the IMF  $B_y$  component beyond the RMP effect. Thus, there is an explicit  $B_y$  effect only in the westward electrojet.

### 5. UT Dependence of the Explicit $B_y$ Effect in $AL$

Figure 11 shows the ratio  $R_{expl}^{+/-}(AL)$  in different months and different UT hours. While the ratio shows qualitatively the same seasonal pattern for all UT hours as in Figure 8, the highest values are found around 5 UT and the lowest values approximately 12 hr later around 17–19 UT. This can be best seen in the right panel,

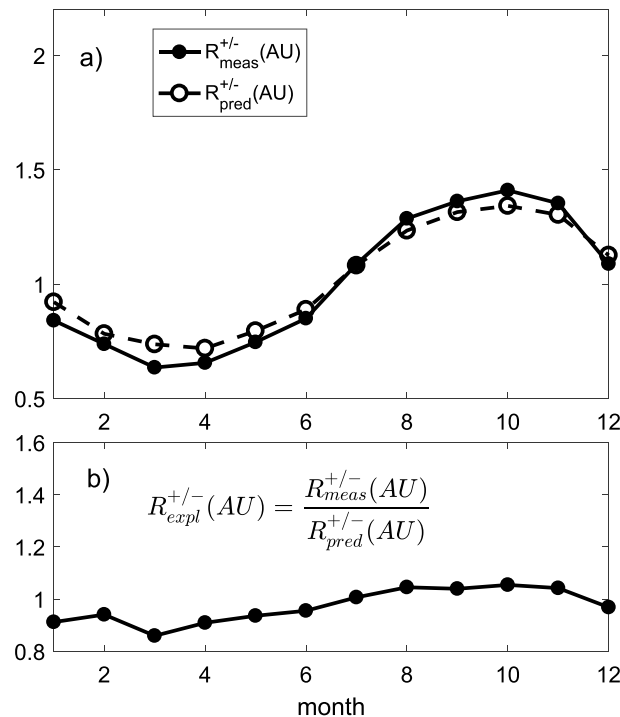


**Figure 10.** (a) Measured and predicted ratios of  $AU(B_y > 0)/AU(B_y < 0)$  [ $R_{meas}^{+/-}(AU)$  and  $R_{pred}^{+/-}(AU)$ , respectively]. (b) Ratio of measured and predicted ratios  $R_{expl}^{+/-}(AU) = R_{meas}^{+/-}(AU)/R_{pred}^{+/-}(AU)$ .

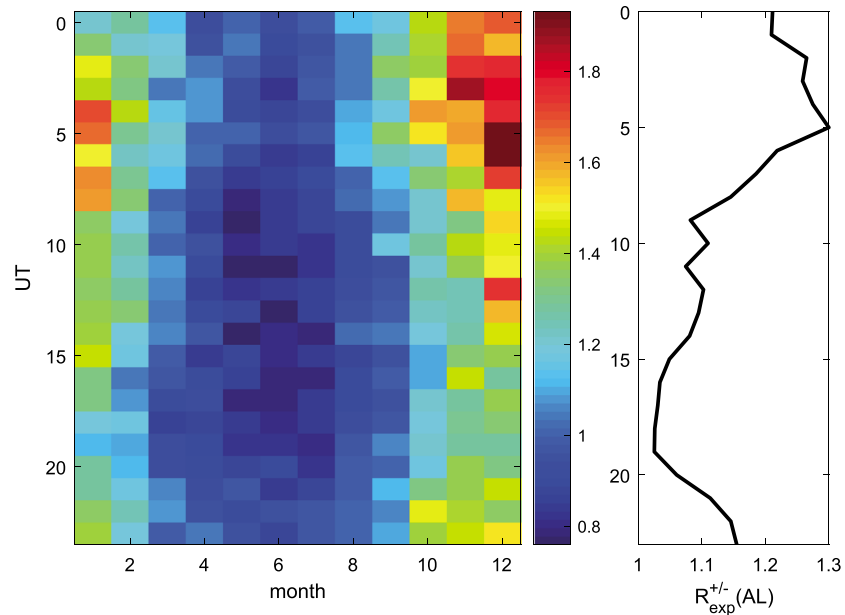


**Figure 11.** (left) Ratio  $R_{\text{expl}}^{+/-}(AL)$  calculated separately in different UT hours and months. (right)  $R_{\text{expl}}^{+/-}(AL)$  in different UT hours averaged over all months. UT = universal time.

which shows the averages of  $R_{\text{expl}}^{+/-}(AL)$  over all 12 months. Interestingly, at 5 UT the Earth’s dipole axis points toward the night sector (antisunward direction) in the NH, while the maximal tilt toward the noon (sunward direction) takes place at 17 UT. This UT variation of  $R_{\text{expl}}^{+/-}(AL)$ , together with its seasonal variation discussed above (see Figure 8), strongly indicate that the explicit  $B_y$  dependence in the AL index is related to (lack of) illumination and is effective when the auroral region of the NH is maximally in darkness.

### 6. IMF $B_y$ Effect in the SH

In order to study whether the explicit  $B_y$  dependence also appears in the high-latitude geomagnetic activity of the SH, we repeat the above analysis using the K index of the Japanese Syowa station. Because the Syowa station is located close to the Southern auroral region, its K index is primarily affected by the auroral electrojets. Since Syowa K index is a local measure of geomagnetic activity, we cannot study the UT variation.

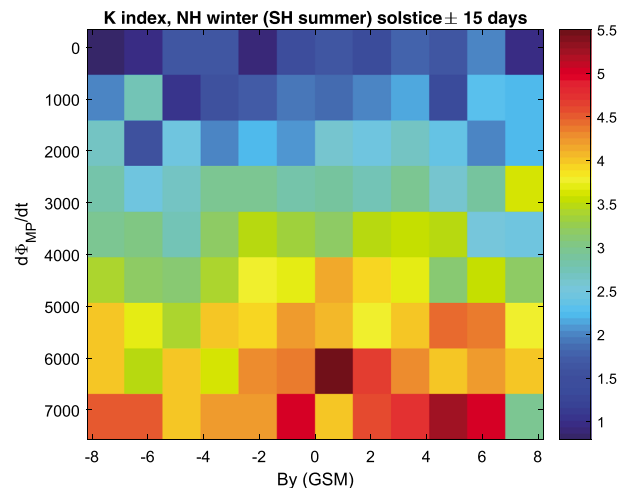


**Figure 12.** Averages of the K index of Syowa station in color code during different levels of  $d\Phi_{\text{MP}}/dt$  and  $B_y$  in Northern Hemisphere (NH) winter (Southern Hemisphere, SH, summer). GSM = geocentric solar magnetospheric.

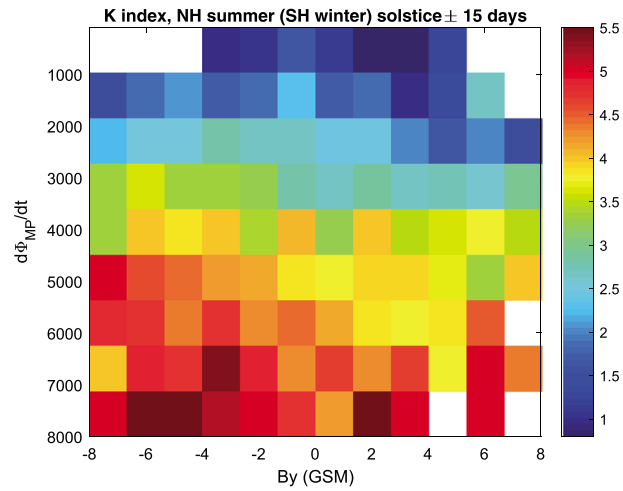


**Figure 13.** Same as Figure 12, but for Northern Hemisphere (NH) summer (Southern Hemisphere, SH, winter).

Here we only use the two 3-hr  $K$  index bins (0–2 UT and 3–6 UT corresponding to 21–23 LT and 0–2 LT) closest to the local midnight sector, where the effect of the westward electrojet is largest.

Figures 12 and 13 show the averages of the Syowa  $K$  index for different values of  $d\Phi_{MP}/dt$  and  $B_y$  in NH winter and summer, or SH summer and winter, respectively, in analogy with Figures 3 and 4 for the  $|AL|$  index. The stronger and more systematic dependence of the Syowa  $K$  index on  $B_y$  polarity is seen during NH summer (SH winter), when geomagnetic activity decreases with  $B_y$  for a given  $d\Phi_{MP}/dt$ . A weaker  $B_y$  dependence is seen during NH winter (SH summer). These effects are further quantified in Figure 14a, which shows the monthly ratios  $R_{meas}^{+/-}(K)$  and  $R_{pred}^{+/-}(K)$ . The predicted values of the  $K$  index are calculated from simultaneous 3-hr averages of  $d\Phi_{MP}/dt$  ( $a = 0.00029 \text{ nT}^{-2/3}/(\text{km/s})^{-4/3}$  and  $b = 1.22$ ). The explicit  $B_y$  dependence of the Syowa  $K$  index is clearly seen in Figure 14b, which shows the ratio  $R_{expl}^{+/-}(K)$ . The explicit  $B_y$  effect maximizes

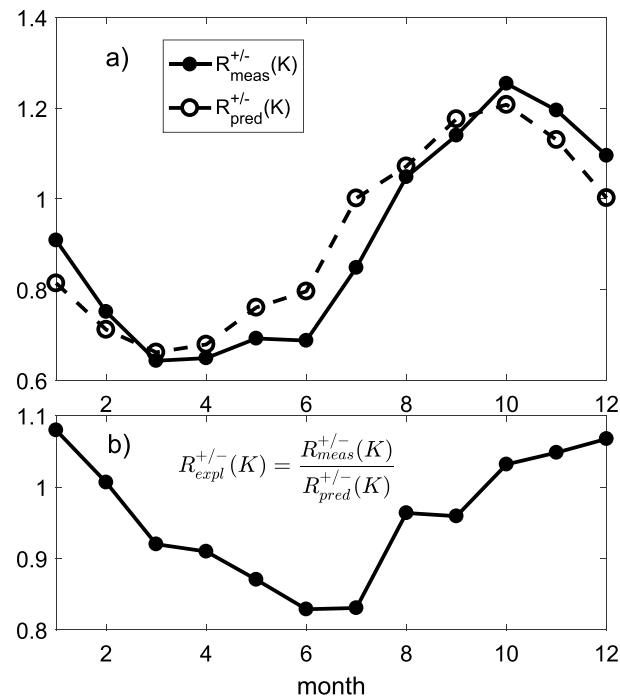


**Figure 14.** (a) Measured and predicted ratios of  $K(B_y > 0)/K(B_y < 0)$  ( $R_{meas}^{+/-}(K)$  and  $R_{pred}^{+/-}(K)$ , respectively). (b) Ratio of measured and predicted ratios  $R_{expl}^{+/-}(K) = R_{meas}^{+/-}(K)/R_{pred}^{+/-}(K)$ .

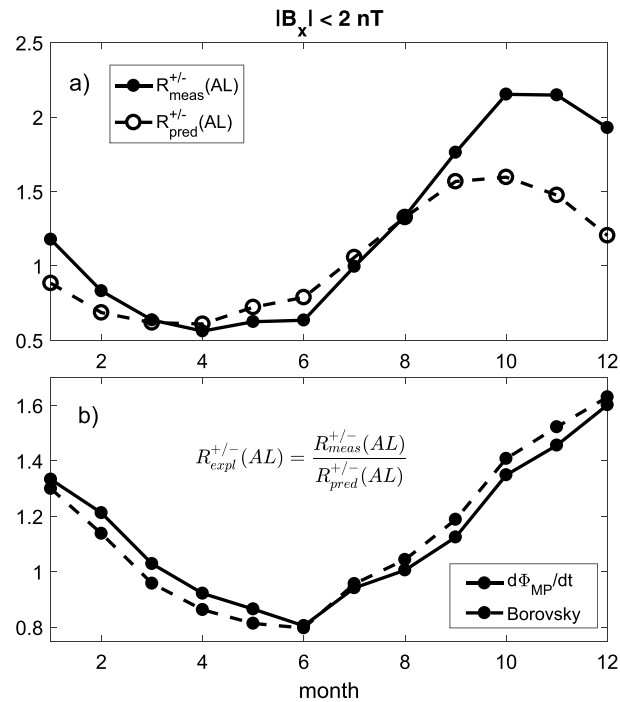


**Figure 15.** Same as Figure 8, but for  $|B_x| < 2$  nT.

during SH winter (in June), when the  $K$  index is suppressed for  $B_y > 0$  and  $R_{expl}^{+/-}(K) = 0.81$ . Thus, the suppression of high-latitude geomagnetic activity in local winter is due to  $B_y > 0$  in SH and  $B_y < 0$  in NH. Figures 12 and 14b also show that in SH summer  $B_y < 0$  leads to a slight suppression of the  $K$  index and  $R_{expl}^{+/-}(K) > 1$ .

The explicit  $B_y$  effect is notably weaker in the (local) Syowa  $K$  index than in the AL index covering a range of longitudes in NH (compare Figures 8b and 14b). The maximum  $B_y$  effect in the Syowa  $K$  index occurs in June, when  $1/R_{expl}^{+/-}(K) \approx 1.22$ , while the maximum of  $R_{expl}^{+/-}(AL)$  in December is about 1.5. Thus,  $R_{meas}^{+/-}(K)$  is 22% smaller than expected from the solar wind coupling function in June, while  $R_{meas}^{+/-}(AL)$  is 50% larger than expected in December. This difference in the magnitude of the explicit  $B_y$  effect is probably due to the UT variation of the  $B_y$  effect, which in the SH is shifted by 12 hr from the UT variation of NH. Thus, the strongest  $B_y$  effect for the SH (around 17 UT) is not observed in the local night sector of Syowa (UT 21–02). Summarizing, there is an opposite explicit  $B_y$  dependence in local winter in the SH, with  $B_y > 0$  conditions leading to suppressed geomagnetic activity.

## 7. Effect of IMF $B_x$

In earlier sections we have quantified the effect of IMF  $B_y$  to high-latitude geomagnetic activity without considering a possible effect of IMF  $B_x$ . Because a typical IMF field line follows the Parker spiral, there is a well-known anticorrelation between  $B_y$  and  $B_x$ . Thus, because  $B_y$  and  $B_x$  are not independent, the analysis in the earlier sections could be biased by  $B_x$ . To test whether effect of IMF  $B_y$  dominates over  $B_x$ , in Figure 15 we repeat the above analysis depicted in Figure 8 under the additional constraint that  $|B_x| < 2$  nT. Because there are no significant differences between Figures 8 and 15, we can conclude that the possible  $B_x$  effect is much weaker than the  $B_y$  effect.

We note that Laundal et al. (2018) found that auroral currents are only weakly ( $\leq 10\%$ ) affected by  $B_x$ . They suggested that the solar wind-magnetosphere coupling is more efficient when the tilt angle of the Earth's magnetic field and  $B_x$  have the same sign, when the reconnection line moves toward subsolar magnetopause (Hoilijoki et al., 2014), making reconnection more efficient. This would lead to strongest geomagnetic activity for  $B_x > 0$  ( $B_x < 0$ ) in NH summer solstice at 17 UT (winter solstice at 5 UT). Thus, the  $B_x$  effect should have similar seasonal/UT variation as the  $B_y$  effect, making the separation of these two effects even more difficult. Detailed future studies are needed for more accurate quantification of  $B_x$  effect and its physical mechanism.

## 8. Discussion and Conclusions

In this paper we have studied how the IMF  $B_y$  component affects to high-latitude geomagnetic activity, using geomagnetic indices from both hemispheres. We have confirmed the earlier observations (Friis-Christensen et al., 2017; Laundal et al., 2016; Smith et al., 2017) that the IMF  $B_y$  polarity and amplitude modulate the strength of the westward electrojet so that the westward electrojet is weaker for  $B_y < 0$  in NH winter and for  $B_y > 0$  in SH winter. We have shown here that this explicit  $B_y$  dependence is not due to the RMP effect or other known effects in the solar wind-magnetosphere coupling (such as the equinoctial effect). We have also demonstrated that the explicit  $B_y$  effect leads to suppression (for  $B_y < 0$ ) rather than enhancement (for  $B_y > 0$ ) of high-latitude geomagnetic activity in NH winter.

Furthermore, we have shown that the explicit  $B_y$  effect depends strongly on UT. The strongest  $B_y$  effect to the  $AL$  index is observed at 5 UT in (NH) winter, when the Earth's dipole axis points toward the night. This UT variation, together with the seasonal variation, verify that the explicit  $B_y$  dependence of high-latitude geomagnetic activity maximizes when the local auroral region is maximally shadowed during local winter solstices.

Ruohoniemi and Greenwald (2005) and Pettigrew et al. (2010) have found that the ionospheric convection in NH (measured by the cross-polar cap potential) is stronger in winter for  $B_y > 0$  and in summer for  $B_y < 0$ . They also found that the IMF  $B_y$  effect is especially strong in the dawn convection cell, which is connected to the westward electrojet. Thus, these studies are in agreement with the order of  $B_y$  dependence and with our finding of a strong  $B_y$  effect in the westward electrojet but not in the eastward electrojet. Friis-Christensen et al. (2017) suggested that  $B_y$  modulates the intensity of the substorm current wedge, possibly explaining the  $B_y$  dependence in the  $AL$  index. Our results imply that the substorm current wedge is suppressed for  $B_y < 0$  in NH winter (rather than enhanced for  $B_y > 0$ ). While this effect is consistent with the observations of this paper, its physical mechanism still remains unknown. Further studies are needed to better understand the physical mechanism behind the explicit  $B_y$  effect in high-latitude geomagnetic activity. The results of this paper are important for understanding and predicting space weather effects at high latitudes and for understanding the connection between long-term geomagnetic activity and solar wind variations.

### Acknowledgments

We acknowledge the financial support by the Academy of Finland to the ReSoLVE Centre of Excellence (project 272157). The solar wind data and the  $AL$  index were downloaded from the OMNI2 database (<http://omniweb.gsfc.nasa.gov/>). The  $K$  index of the Syowa station was downloaded from the National Institute of the Polar Research, Japan at <http://polaris.nipr.ac.jp>.

### References

- Borovsky, J. E., & Birn, J. (2014). The solar wind electric field does not control the dayside reconnection rate. *Journal of Geophysical Research: Space Physics*, 119, 751–760. <https://doi.org/10.1002/2013JA019193>
- Cliver, E. W., Kamide, Y., & Ling, A. G. (2000). Mountains versus valleys: Semiannual variation of geomagnetic activity. *Journal of Geophysical Research*, 105(A2), 2413–2424. <https://doi.org/10.1029/1999JA900439>
- Davis, T. N., & Sugiura, M. (1966). Auroral electrojet activity index AE and its universal time variations. *Journal of Geophysical Research*, 71(3), 785–801.
- Dungey, J. W. (1961). Interplanetary magnetic field and the auroral zones. *Physical Review Letters*, 6, 47–48.
- Finch, I. D., Lockwood, M. L., & Rouillard, A. P. (2008). Effects of solar wind magnetosphere coupling recorded at different geomagnetic latitudes: Separation of directly-driven and storage/release systems. *Geophysical Research Letters*, 35, L21105. <https://doi.org/10.1029/2008GL035399>
- Friis-Christensen, E., Finlay, C. C., Hesse, M., & Laundal, K. M. (2017). Magnetic field perturbations from currents in the dark polar regions during quiet geomagnetic conditions. *Space Science Reviews*, 206(1–4), 281–297.
- Friis-Christensen, E., Kamide, Y., Richmond, A. D., & Matsushita, S. (1985). Interplanetary magnetic field control of high-latitude electric fields and currents determined from Greenland magnetometer data. *Journal of Geophysical Research*, 90(A2), 1325–1338. <https://doi.org/10.1029/JA090iA02p01325>
- Friis-Christensen, E., Lassen, K., Wilhelm, J., Wilcox, J. M., Gonzalez, W., & Colburn, D. S. (1972). Critical component of the interplanetary magnetic field responsible for large geomagnetic effects in the polar cap. *Journal of Geophysical Research*, 77(19), 3371–3376. <https://doi.org/10.1029/JA077i019p03371>
- Holljoki, S., Souza, V. M., Walsh, B. M., Janhunen, P., & Palmroth, M. (2014). Magnetopause reconnection and energy conversion as influenced by the dipole tilt and the IMF  $B_x$ . *Journal of Geophysical Research: Space Physics*, 119, 4484–4494. <https://doi.org/10.1002/2013JA019693>
- Kan, J. R., & Lee, L. C. (1979). Energy coupling function and solar wind-magnetosphere dynamo. *Geophysical Research Letters*, 6(7), 577–580. <https://doi.org/10.1029/GL006i007p00577>
- Laundal, K. M., Gjerloev, J. W., Ostgaard, N., Reistad, J. P., Haaland, S., Snekvik, K., et al. (2016). The impact of sunlight on high-latitude equivalent currents. *Journal of Geophysical Research: Space Physics*, 121, 2715–2726. <https://doi.org/10.1002/2015JA022236>
- Laundal, K. M., Reistad, J. P., Finlay, C. C., Østgaard, N., Tenfjord, P., Snekvik, K., & Ohma, A. (2018). Interplanetary magnetic field  $B_x$  component influence on horizontal and field-aligned currents in the ionosphere. *Journal of Geophysical Research: Space Physics*, 123. <https://doi.org/10.1002/2017JA024864>
- Lyatsky, W., Newell, P. T., & Hamza, A. (2001). Solar illumination as cause of the equinoctial preference for geomagnetic activity. *Geophysical Research Letters*, 28(12), 2353–2356. <https://doi.org/10.1029/2000GL012803>
- Mansurov, S. M. (1969). New evidence of a relationship between magnetic fields in space and on Earth. *Geomagnetism and Aeronomy*, 9, 622–624.
- Newell, P. T., Sotirelis, T., Liou, K., Meng, C.-I., & Rich, F. J. (2007). A nearly universal solar wind-magnetosphere coupling function inferred from 10 magnetospheric state variables. *Journal of Geophysical Research*, 112, A01206. <https://doi.org/10.1029/2006JA012015>

- Pettigrew, E. D., Shepherd, S. G., & Ruohoniemi, J. M. (2010). Climatological patterns of high-latitude convection in the Northern and Southern Hemispheres: Dipole tilt dependencies and interhemispheric comparisons. *Journal of Geophysical Research*, *115*, A07305. <https://doi.org/10.1029/2009JA014956>
- Ruohoniemi, J. M., & Greenwald, R. A. (1996). Statistical patterns of high-latitude convection obtained from Goose Bay HF radar observations. *Journal of Geophysical Research*, *101*(A10), 21,743–21,763. <https://doi.org/10.1029/96JA01584>
- Ruohoniemi, J. M., & Greenwald, R. A. (2005). Dependencies of high-latitude plasma convection: Consideration of interplanetary magnetic field, seasonal, and universal time factors in statistical patterns. *Journal of Geophysical Research*, *110*, A09204. <https://doi.org/10.1029/2004JA010815>
- Russell, C. T., & McPherron, R. L. (1973). Semiannual variation of geomagnetic activity. *Journal of Geophysical Research*, *78*(1), 92–108.
- Smith, A. R. A., Beggan, C. D., Macmillan, S., & Whaler, K. A. (2017). *Climatology of the auroral electrojets derived from the along-track gradient of magnetic field intensity measured by POGO, Magsat, CHAMP, and Swarm* (Vol. 15). <https://doi.org/10.1002/2017SW001675>
- Svalgaard, L. (1968). Sector structure of the interplanetary magnetic field and daily variation of the geomagnetic field at high latitudes (Geophysical Papers R-6). Copenhagen, Denmark: Danish Meteorological Institute.